Kamil, G. M., Liang, Q. Q. and Hadi, M. N. S. (2019). Numerical analysis of axially loaded rectangular concrete-filled steel tubular short columns at elevated temperatures. *Engineering Structures*, 180: 89-102.

Numerical analysis of axially loaded rectangular concrete-filled steel tubular short columns at elevated temperatures

Ghanim Mohammed Kamil[a], Qing Quan Liang[a,*], Muhammad N. S. Hadi[b]

[a] *College of Engineering and Science, Victoria University, PO Box 14428, Melbourne, VIC 8001, Australia*

[b] *School of Civil, Mining and Environmental Engineering, University of Wollongong, Wollongong, NSW 2522, Australia*

Abstract

Elevated temperatures significantly reduce the local buckling strengths of steel tubes and the ultimate strengths of rectangular concrete-filled steel tubular (CFST) columns exposed to fire. No fiber-based models have been developed that include local buckling effects on the fire-resistance of rectangular CFST columns. This paper presents a new fiber element model for the fire-resistance predictions of axially loaded rectangular CFST short columns at elevated temperatures considering local buckling. The thermal analysis problem of a CFST column is solved by the finite difference method to determine the temperature distribution within its cross-section including an air gap, concrete moisture content and the emissivity of exposure surfaces. The nonlinear stress analysis of axially loaded short CFST columns under fire recognizes the stress-strain behavior of concrete and steel at elevated temperatures. The expressions for initial local buckling and effective widths of steel plates are incorporated in the computational model to include the effects of local and post-local buckling on the fire responses of CFST columns. The existing experimental and numerical results are utilized to examine the accuracy of the fiber-based model. The fiber model developed is used to undertake parametric studies on the

* Corresponding author. Tel.: 61 3 9919 4134.
E-mail address: Qing.Liang@vu.edu.au (Q. Q. Liang)

effects of local buckling, geometric and material properties and loading ratio on the thermal and structural responses of CFST short columns and the load distribution in steel tube and concrete. The numerical model proposed is demonstrated to simulate well the fire and structural performance of axially loaded CFST short columns under fire. Moreover, computational solutions presented provide a better understanding of the thermal and structural responses of CFST columns in fire.

Keywords: Concrete-filled steel tubes; Elevated temperatures; Fire-resistance; Nonlinear analysis; Local buckling.

1. Introduction

Rectangular concrete-filled steel tubular (CFST) columns have been widely used to resist heavy loads in high-rise composite buildings. Filling a rectangular hollow steel tube with concrete as illustrated in Fig. 1 not only remarkably increases the strength and stiffness of the hollow steel tube but also significantly improves its fire-resistance. The concrete infill is completely encased by the rectangular steel tube so that it exhibits improved ductility. In addition, the steel tube acts as longitudinal reinforcement and permanent formwork for the filled concrete, which greatly reduces the construction time and costs. Moreover, the concrete core delays the steel tube local buckling and forces it to buckle locally outward [1-9]. Some of the practical applications of circular and rectangular/square CFST columns in high-rise buildings include LDC Queen's Road Central in Hong Kong, Di Wang and The SEG Plaza in Shenzhen, the Sail in Singapore, the Petronas Tower in Kuala Lumpur and Two Union Square in Seattle. In AS 3600-2009 [10], columns with a slenderness ratio (L/r) less than 22 are regarded as short columns. As shown in Table 1, the sizes of CFST columns used in the above mentioned high-rise buildings were very large and their slenderness ratios calculated by assuming the typical

story height of 4.2 m ranged from 5.3 to 17.7. These CFST columns therefore were short columns whose strengths were governed by the section capacities. Rectangular CFST columns in tall composite structures may be exposed to extreme events such as fire in their design life. The elevated temperatures generated in a fire significantly reduce the stiffness and strength of concrete and steel materials as well as the local buckling resistance of steel tubes and therefore the ultimate strengths of CFST columns [11-13]. To accurately determine the fire-resistance of rectangular CFST columns, the influences of local buckling must be included in the nonlinear analysis procedures. However, no fiber-based modeling techniques have been proposed that included local buckling in the fire-resistance prediction of CFST short columns. Therefore, there is a need for the development of such a computational technique.

Most of the experimental investigations on the fire-performance of CFST columns have focused on slender columns. Standard fire tests on square, rectangular and circular CFST slender columns subjected to constant axial load and increasing temperatures that followed the standard temperature-time curve given in design codes have been conducted by researchers, such as Lie and Chabot [14], Sakumoto et al. [15], Kodur and Lie [16], Han et al. [17], Choi et al. [18], Han et al. [19], Espinos et al. [20,21], and Dundu [22]. The temperatures on the surfaces and in the column cross-section, the axial deformation and the fire-resistance of the CFST column were recorded in the fire tests. The effects of important parameters were investigated, including the axial load ratio, loading eccentricity, column slenderness and size, types of concrete infill, material strengths and spray material thickness. Experimental results indicated that the typical failure mode associated with slender CFST columns in fire was overall column buckling. For CFST rectangular and square columns, however, the steel tube buckled locally outward.

Experimental studies on the responses of short square and rectangular CFST columns exposed to fire have been extremely scarce. Lu et al. [23] carried out fire tests on short CFST columns constructed by high-strength self-consolidating concrete to determine the temperature distributions, axial displacement-time relationships, limiting temperatures and fire-resistance. It was reported that the outward local buckling appeared on the four faces of each column while the concrete crushed at the column where the steel tube walls locally buckled. In addition, the axial load ratio had significant influences on the fire-performance of short square CFST columns. Moreover, the loading eccentricity was shown to have a minor effect on the fire-resistance of short CFST columns. Furthermore, it was observed that there was an interaction between the steel tube and concrete infill during the fire exposure.

Although fire tests can be performed to determine the responses of CFT columns exposed to fire, these tests are highly time consuming and expensive. Therefore, mathematical models have been formulated for the fire-resistance predictions of CFST slender columns by researchers. The fiber-based numerical models for simulating the responses of slender CFST columns exposed to fire have been developed by Lie and Chabot [24], Lie and Irwin [25] and Kodur and Lie [26], Han [27], and Chung et al. [28]. In these fiber-based models, either the finite difference or the finite element method was utilized to calculate the distribution of temperatures in the column considering concrete and steel thermal properties. The numerical models considered the nonlinear stress-strain characteristics of concrete as well as steel at elevated temperatures, moisture in concrete, second order effects as well as geometric imperfections. Researchers have also employed commercial finite element software ABAQUS and ANSYS to create 3D models to investigate the responses of CFST slender columns in fire [29-33]. Ding and Wang [29] and Espinos et al. [30] examined the influences of the air gap, slip at the concrete and steel tube interface, tensile concrete strength and geometric imperfection on the fire-resistance of CFST

columns. Hong and Varma [31] carried out extensive sensitivity analyses on the influences of material constitutive models, geometric imperfections, local buckling and the bond between the steel tube and concrete on the performance of square CFST columns.

Numerical studies on rectangular short CFST columns at elevated temperatures have been relatively limited. Yin et al. [34] presented an analytical model for the fire-performance predictions of square and circular CFST short column subjected to axial load and fire. It was reported that for the same concrete and steel cross-sectional areas, circular CFST short columns had slightly higher fire-resistance than square ones. The axial load-deformation responses of short CFST square and circular columns subjected to combined axial load and elevated temperatures including a cooling phase were investigated by Song et al. [35] using ABAQUS. The stress distributions and confinement stresses at different loading stages were also studied. The finite element results indicated that heating slightly increased the ultimate load of CFST circular columns but reduced that of square ones. Dai and Lam [36] utilized ABAQUS to examine the influences of the column sectional shape on the thermal and structural behavior of CFST short columns made of circular, elliptical, square or rectangular sections at elevated temperatures. The results obtained demonstrated that circular CFST short columns had higher fire performance than other sections. Increasing the axial load ratio remarkably reduced the critical temperatures and fire-resistance of CFST short columns regardless of sectional shape. The distribution of temperatures in CFST columns constructed by carbon or stainless steel tubes was investigated using ABAQUS by Tao and Ghannam [37], who reported that the thermal contact conductance at the interface of steel and concrete and concrete moisture content significantly influenced the temperature distribution. Xiong et al. [38] presented a modified finite difference method for computing the temperature distributions in circular and square CFST columns and in double-skin CFST columns exposed to fire. The numerical model

presented was employed to undertake sensitivity analyses on the influences of important factors on the responses of CFST columns at elevated temperatures.

It appears from the above literature review that the existing fiber-based numerical models have not considered local buckling effects in the analysis of rectangular CFST columns under fire. Although local buckling could be included in the finite element analysis of rectangular CFST columns in fire, the development and computational cost of the finite element model is highly expensive compared to that of the fiber element model [31,39]. The comparative study conducted by Ahmed et al. [39] demonstrated that the total time for creating and analyzing the finite element model of a concrete-filled double steel tubular short column was 2640 s while the total time for creating and analyzing its fiber element model was only 25 s. Moreover, there are relatively limited studies dealing with rectangular short CFST columns under fire loading. To address this knowledge gap, this paper describes a computationally efficient fiber-based numerical model for simulating the thermal and structural behaviors of axially-loaded short CFST rectangular columns subjected to elevated temperatures. The fiber model includes the influences of local and post-local buckling of steel tube, air gap, moisture content and emissivity of exposure surfaces on the fire performance of CFST columns. The mathematical formulations of the numerical model are described and its verification is followed. The fiber modeling technique is utilized to undertake a parametric study on the fire and structural responses of CFST columns with various important parameters.

2. The fiber element model for thermal problems

2.1 Discretization of cross-section

The present numerical model is developed using the fiber element method, which discretizes the cross-section of a CFST column into many small fiber elements but it does not require any discretization along the column length [40-44]. A typical fiber mesh of the column cross-section is depicted in Fig. 2 where the section is formed by welding four plates without the corner radius. The wall of the steel tube is discretized into layers through its thickness while its width is divided into square fiber elements according to the layer thickness. The filled concrete is discretized into square fiber elements and the size of the concrete fiber is twice the size of the steel fiber element as illustrated in Fig. 2. The temperature at the center of each fiber element is taken as its temperature. The material properties of steel or concrete are assigned to fibers. The uniaxial material stress-strain relationships of steel and concrete at elevated temperatures are employed to compute fiber stresses from axial fiber strains.

2.2 The sequential coupled analysis procedure

The nonlinear inelastic analysis of CFST short columns exposed to fire consists of sequential coupled thermal analysis and nonlinear stress analysis. In the thermal analysis, the temperatures on surfaces of the CFST column as a function of time are calculated first. The distribution of temperatures in the column cross-section is then computed by numerical techniques. The temperature is assigned to each fiber element based on the computed temperature distribution. The nonlinear stress analysis is carried out to simulate the structural responses of the axially loaded CFST short column under elevated temperatures determined in the thermal analysis. For a given time increment, the temperatures on the surfaces of the CFST column and within its cross-section are computed. The axial strain is incrementally increased and the corresponding axial load is computed as stress resultants in the section subjected to the computed temperature distribution. By repeating the above analysis process, the axial load-strain curves for the CFST short column for given time increments of fire exposure can be determined. The ultimate axial

strength of the CFST column decreases as time increases. The fire-resistance of the CFST short column is determined as the time to reach the failure point of the column which has so low strength that it cannot support the axial load. A computer program implementing the fiber-based numerical model has been developed using MATLAB by the authors. The thermal and the nonlinear stress analyses are described in the following sections.

3. Thermal analysis

3.1. Fire temperature-time relationship

The standard temperature-time curve given in Eurocode 1 [45] as demonstrated in Fig. 3 is adopted in the present fiber model to determine the temperatures on the surfaces of the CFST column during fire exposure. This standard curve is expressed by

$$T(t) = 20 + 345log_{10}(8t + 1) \tag{1}$$

where T stands for the temperature in $^{\circ}C$ and t is the time of fire exposure in minutes.

3.2. Temperature distribution in the cross-section

The four sides of the rectangular CFST column are assumed to be exposed to uniform temperatures that follow the standard temperature-time curve represented by Eq. (1). To determine the temperature distribution at the fiber elements in the cross-section, the finite difference method is employed to solve the following heat transfer equation in two-dimensions [46]:

$$k\frac{\partial^2 T}{\partial x^2}+k\frac{\partial^2 T}{\partial y^2}+q=\rho c\frac{\partial T}{\partial t} \tag{2}$$

where ρ denotes the density in $\mathrm{kg/m^3}$, c is the specific heat in $\mathrm{J/kg}$, and k is the thermal conductivity in $\mathrm{W/m^{\circ}C}$ and q is the heat flux which is used to calculate the temperature distribution on the surfaces of the CFST column but is taken as zero for steel and concrete within the column.

The thermal properties of steel and concrete including the thermal conductivity, specific heats and thermal expansion coefficient need to be specified in the thermal analysis. The thermal properties of steel provided in Eurocode 3 [47] and the thermal properties of concrete given by Lie and Chabot [24] are employed in the fiber-based numerical model and are provided in Table 2 for convenience and completeness.

The nodes of fiber elements in the cross-section are schematically illustrated in Fig. 4. The distances between the adjacent two nodes in *x* and *y* directions are represented by *dx* and *dy*, respectively, and they are actually the size of the fiber element in *x* and *y* directions, respectively. As shown in Fig. 4, *m* and *n* denote the coordinates of the node in the *y* and *x* directions, respectively. Assume that the current temperature at the node (*m*, *n*) at the *i*th time increment is $T_{m,n}^{i}$. The next temperature $T_{m,n}^{i+1}$ at this node at the next time increment is calculated by solving the general heat transfer equation expressed by Eq. (2) using the forward finite difference method as follows:

$$T_{m,n}^{i+1}=\frac{\alpha\Delta t}{(\Delta L)^2}\left(T_{m,n-1}^{i}+T_{m,n+1}^{i}+T_{m-1,n}^{i}+T_{m+1,n}^{i}\right)+\left(1-\frac{4\alpha\Delta t}{(\Delta L)^2}\right)T_{m,n}^{i} \tag{3}$$

in which $1-(4\alpha\Delta t/\Delta L)^2 \geq 0$; α is the diffusivity and is taken as $k/\rho c$; Δt is the time step in seconds; and the distance between two adjacent nodes is $\Delta L = dx = dy$.

It is assumed that an air gap between the steel tube and concrete during fire exposure exists because the steel tube expanses more than the filled concrete does [29]. The temperatures at the contact nodes at the steel and concrete interface are computed by the following equation accounting for the effects of the air gap where the thermal contact resistance h_{tr} is taken as 100 $\mathrm{W/m^2K}$ as suggested by other researchers [29]:

$$T_{1,1}^{i+1} = T_{1,1}^{i} + \frac{4\Delta t}{\rho c\left(dc\right)^2}\left(h_{tr}(T_{3,3}^{i} - T_{1,1}^{i})dc + \lambda_c(T_{1,2}^{i} - T_{1,1}^{i}) + \lambda_c(T_{2,1}^{i} - T_{1,1}^{i})\right) \quad (4)$$

where d_c and d_s are the concrete and steel fiber sizes, respectively, and the symbols that refer to the temperatures at nodes used in the above equation are illustrated in Fig. 5 , which shows the interaction nodes between steel and concrete at the corner of the interface of steel and concrete as a typical case. The temperatures at the nodes of steel fibers at the boundaries can be calculated by using Eq. (4) with the heat convection and thermal radiation coefficients. Research studies on the thermal analysis of CFST columns showed that the emissivity of the exposure surfaces and the moisture content in concrete had remarkable effects on the distribution of temperatures [30,31]. In the present numerical model, the emissivity of the exposure surface ($\widehat{\varepsilon}$) is taken as 0.7 and the Stephen–Boltzmann constant is taken as 5.67×10^{-8} $\mathrm{W/m^2\ K^4}$, while the moisture content is taken as 3%. These values have been used by other researchers and showed to give good predictions. The use of 3% moisture content is based on Eurocode 2 [48] that limits the moisture content to 3% and the research conducted by Espinos et al. [30]. The research conducted by Tao and Ghannam [37] indicated that the use of

moisture content higher than 3% resulted in the overestimation of the fire-resistance of CFST columns.

To validate the accuracy of the fiber modeling technique for thermal analysis on CFST rectangular columns, computed temperatures at various locations depicted in Fig. 6 are compared with experimentally measured ones provided by Lie and Chabot [14] in Figs. 7-9. The thermal analysis of three square CFST columns tested by Lie and Chabot [14] were undertaken by the proposed fiber model. The dimensions of the column cross sections were 152.4×152.4 mm, 254×254 mm and 304×304 mm while the thickness of the steel tubes was 6.35 mm. It can be observed from these figures that the fiber model predicts well the temperatures at Point 1 on the surface of the column and at Point 2 within the column, but slightly underestimates the temperature at the center of the section. The steel temperature increased rapidly during the first 30 minutes exposure to fire as oppositely to the concrete core due to the direct contact between the steel and the fire source and because the steel has a higher thermal conductivity than concrete, which was protected by steel. The discrepancy between the numerical predictions and measurements of the concrete temperatures was attributed to the uncertainty of the actual thermal properties of concrete. The plateau at concrete temperatures occurred after 30 minutes of fire exposure was caused by the slow rate defined by the standard fire curve and the position of core concrete and the low thermal conductivity of concrete. For the column with a larger cross-section, the Points 2 and 3 at the concrete were farther away from the fire source so that the concrete temperatures at Points 2 and 3 were lower and the curves look plateau as depicted in Figs. 6-8. The maximum temperatures on steel surface and at the core concrete computed by the proposed fiber model are compared against the finite element results obtained by Dai and Lam [36] using ABAQUS in Fig. 10. It appears that excellent agreement between these numerical predictions is obtained.

4. Nonlinear stress analysis

4.1. Axial strains

The short rectangular CFST column is under constant axial compression and increasing temperatures during fire exposure. The strain in steel or concrete consists of axial strain caused by axial load and thermal strain due to thermal expansion. The concrete and steel components in a short CFST column are subjected to the same axial strain (ε). The strain in steel fibers (ε_s) is expressed by

$$\varepsilon_s = \varepsilon - \varepsilon_{s,T} \tag{5}$$

The strain in concrete fibers (ε_c) is calculated as

$$\varepsilon_c = \varepsilon - \varepsilon_{c,T} \tag{6}$$

In the nonlinear stress analysis, the axial strain ε is incrementally increased to determine the corresponding axial load that causes this axial deformation.

4.2. Stress-strain model for steel at elevated temperatures

The stress-strain model for structural steels at elevated temperatures provided in Eurocode 3 [47] is incorporated in the present mathematical model for steels exposed to fire. The stress-strain curves of steels are presented in Fig. 11 and expressed by the following equation:

$$\sigma_{s,T}=\begin{cases} E_T\varepsilon_s & \text{for } \varepsilon_s \le \varepsilon_{p,T} \\ \left(f_{p,T}-h_3\right)+\dfrac{h_2}{h_1}\sqrt{h_1^{\,2}-\left(\varepsilon_{y,T}-\varepsilon_s\right)^2} & \text{for } \varepsilon_{p,T} < \varepsilon_s \le \varepsilon_{y,T} \\ f_{y,T} & \text{for } \varepsilon_{y,T} < \varepsilon_s \le \varepsilon_{t,T} \\ f_{y,T}\left[1-\left(\varepsilon_s-\varepsilon_{t,T}\right)/\left(\varepsilon_{u,T}-\varepsilon_{t,T}\right)\right] & \text{for } \varepsilon_{t,T} < \varepsilon_s \le \varepsilon_{u,T} \\ 0 & \text{for } \varepsilon_s > \varepsilon_{uT} \end{cases} \tag{7}$$

where the coefficients h_1, h_2, and h_3 are given as

$$h_1^{\,2}=(\varepsilon_{y,T}-\varepsilon_{p,T})(\varepsilon_{y,T}-\varepsilon_{p,T}+h_3/E_T) \tag{8}$$

$$h_2^{\,2}=E_T(\varepsilon_{y,T}-\varepsilon_{p,T})h_3+h_3^{\,2} \tag{9}$$

$$h_3=\frac{(f_{y,T}-f_{p,T})^2}{E_T\ (\varepsilon_{y,T}-\varepsilon_{p,T})-2\ (f_{y,T}-f_{p,T})} \tag{10}$$

where E_T denotes the elastic modulus for steel, $f_{p,T}$ stands for the proportional limit, $f_{y,T}$ represents the yield stress, $\varepsilon_{p,T}$ is the strain at $f_{p,T}$, $\varepsilon_{y,T}$ denotes the yield strain, and $\varepsilon_{u,T}$ stands for the ultimate strain at elevated temperatures. The reduction factors $R_{p,T}$ to the proportional limit, $R_{y,T}$ to the steel yield strength and $R_{E,T}$ to the modulus of elasticity of steels at elevated temperatures provided in Eurocode 3 [47] are used in the present study and are shown in Fig. 12.

The strain-hardening of steel at temperatures below $400^{\circ}\mathrm{C}$ is taken into consideration by the following expression [47]:

$$\sigma_{s,T}=\begin{cases}50\left[\left(f_{u,T}-f_{y,T}\right)/0.02\right]+2f_{y,T}-f_{u,T} & \text{for } 0.02<\varepsilon_s\le 0.04\\ f_{u,T} & \text{for } 0.04<\varepsilon_s\le 0.15\\ f_{u,T}\left[1-20\left(\varepsilon_s-0.15\right)\right] & \text{for } 0.15<\varepsilon_s\le 0.2\end{cases} \quad (11)$$

where $f_{u,T}$ denotes the ultimate strength of steel at elevated temperature, which is calculated as follows:

$$f_{u,T}=\begin{cases}f_u R_{y,T} & \text{for } T\le 300^{\circ}C\\ f_{y,T}+0.01\left(f_{u,T}-f_{y,T}\right)\left(400-T\right) & \text{for } 300<T\le 400^{\circ}C\end{cases} \quad (12)$$

4.3. Stress-strain model for concrete at elevated temperatures

For concrete at elevated temperatures, the stress-strain model given in Eurocode 2 [48] is incorporated in the numerical model and illustrated in Fig. 13. This model is represented by the following equation:

$$\sigma_{c,T}=\begin{cases}\dfrac{3\varepsilon_c f'_{c,T}}{\varepsilon'_{c,T}\left[2+\left(\varepsilon_c/\varepsilon'_{c,T}\right)^3\right]} & \text{for } \varepsilon_c\le\varepsilon'_{c,T}\\ f'_{c,T}\left[\dfrac{\varepsilon_{cu,T}-\varepsilon_c}{\varepsilon_{cu,T}-\varepsilon'_{c,T}}\right] & \text{for } \varepsilon_c>\varepsilon'_{c,T}\end{cases} \quad (13)$$

where $f'_{c,T}$ represents the concrete compressive strength, $\varepsilon'_{c,T}$ denotes the concrete strain at $f'_{c,T}$, and $\varepsilon_{cu,T}$ is the concrete ultimate strain at elevated temperatures. The concrete strain values of $\varepsilon'_{c,T}$ and $\varepsilon_{cu,T}$ at elevated temperatures can be found in Eurocode 2 [48] for siliceous aggregates and appropriate values should be used for other types of aggregates.

4.4. Critical local buckling of steel tube

The steel tube of a rectangular CFST short column subjected to axial compression are under uniform compression and may undergo outward local buckling [40-42]. Expressions for computing the critical local buckling stress of clamped steel plates in CFST rectangular columns at room temperatures have been proposed by Liang et al. [49]. Liang [40,41] incorporated these expressions in the fiber-based computational model to include local buckling in the nonlinear modeling of CFST columns. The local buckling behavior of steel plates with imperfections at elevated temperatures in CFST rectangular columns was studied by Kamil et al. [50]. Design equations derived by Kamil et al. [50] are included in the present fiber modeling technique to compute the critical local buckling strength of steel tube in axially loaded CFST columns at elevated temperatures. These equations are applicable to steel tube walls with clear width-to-thickness ratio (b / t_s) ranging from 30 to 110.

For a steel tube wall exposed to temperatures ranging from 550 to 650°C, its critical local buckling stress is calculated by [50]

$$\frac{\sigma_{1c,T}}{f_{y,T}} = \left(0.1916\lambda_{c,T}^{-0.7661} + 0.003889\right)\ \left(m_1\lambda_{c,T}^2 + m_2\lambda_{c,T} + m_3\right) \tag{14}$$

where $\sigma_{1c,T}$ stands for the plate critical local buckling stress at elevated temperatures, and λ_{cT} represents the relative slenderness of the plate at elevated temperatures, determined by

$$\lambda_{c,T} = \sqrt{\frac{12(1-\nu^2)(b/t_s)^2(k_{y,T}f_y)}{k\pi^2(k_{E,T}E)}} \tag{15}$$

where f_y denotes the steel yield stress at ambient temperature, ν represents the Poisson's ratio of steel, E is the Young's modulus of steel at ambient temperature, $k = 9.95$ stands for the coefficient of elastic local buckling. The four edges of the steel tube wall in a CFST column are assumed to be clamped as discussed by Liang et al. [49].

The coefficients m_1, m_2 and m_3 in Eq. (14) are given as

$$m_1 = -1.0685\alpha_s^2 + 2.275\alpha_s - 0.8969 \tag{16}$$

$$m_2 = 2.3075\alpha_s^2 - 4.7791\alpha_s + 1.8475 \tag{17}$$

$$m_3 = -0.825\alpha_s^2 + 1.086\alpha_s + 1.0083 \tag{18}$$

where α_s is the stress gradient coefficient and defined as the ratio of the minimum stress to the maximum stress applied to the plate. For CFST columns in axial compression, the steel tube is under uniform edge stresses so that α_s is taken as 1.0.

Expression for predicting the critical local buckling stress of steel plates for any other temperatures given proposed by Kamil et al. [50] is

$$\frac{\sigma_{1c,T}}{f_{y,T}} = (g_1\lambda_{c,T}^{g} + g_2)\frac{0.6566\lambda_{c,T}^{0.001521}\left(\frac{R_{p,T}}{R_{y,T}}\right)^{-0.1598}}{0.5415\lambda_{c,T}^{4.889} + \left(\frac{R_{p,T}}{R_{y,T}}\right)^{-0.8252}} \tag{19}$$

where the coefficients g, g_1 and g_2 are

$$g = -7.9339\,\alpha^2 + 11.29\,\alpha + 4.701 \tag{20}$$

$$g_1 = 0.0863\,\alpha^2 - 0.1248\,\alpha + 0.0431 \tag{21}$$

$$g_2 = 0.2656\,\alpha^2 - 0.9902\,\alpha + 1.719 \tag{22}$$

4.5. Post-local buckling of steel tube

The effective width models developed by Liang et al. [49] were included in the fiber-based computational procedures to take into account the influences of post-local buckling on the performance of CFST columns at room temperatures by Liang [40,41]. The effective widths of a rectangular steel tube in CFST column in axial compression are schematically illustrated in Fig. 14. Kamil et al. [50] formulated effective width equations for computing the post-local buckling strengths of steel plates at elevated temperatures and are applicable to steel tube walls with clear width-to-thickness ratio (b / t_s) ranging from 30 to 110. The development of these formulas considered residual stresses and initial geometric imperfections for temperatures under 400°C were considered in the development of these formulas. The formulas given by Kamil et al. [50] are coded in the computer program for the calculation of the effective widths of steel tube in axially-loaded steel tube in CFST columns in fire, which are expressed by

$$\frac{b_e}{b} = (q_1 \lambda_{c,T}^{q}) \frac{0.8418 \lambda_{c,T}^{0.02368} \left(\frac{R_{p,T}}{R_{y,T}} \right)^{-0.3028} + 1.154 \left(\frac{R_{p,T}}{R_{y,T}} \right)}{2.055 + \lambda_{c,T}^{1.68}} \tag{23}$$

in which b_e and b represent the effective width and clear width of the steel tube wall, respectively; and q and q_1 are expressed by

$$q = 0.04007\alpha_s^2 - 0.05275\alpha_s + 0.03355 \quad (24)$$

$$q_1 = 0.1007\alpha_s^2 - 0.7027\alpha_s + 1.65 \quad (25)$$

After the critical local buckling occurs, the post-local buckling is associated with the redistribution of in-plane stresses in the thin steel plate as discussed by Liang [40,42]. Based on the effective width concept, the steel fiber stresses within the effective widths as illustrated in Fig. 14 are assigned to the steel yield stress while those located in the ineffective widths are set to zero. The simulation of the progressive post-local buckling is undertaken by the gradual redistribution of the in-plane stresses in the buckled steel plate. The effective width of the plate under edge stress greater than its critical buckling stress and less than its ultimate strength is computed by linear integration based on the stress level as suggested by Liang [40]. The modeling procedure given by Liang [40] is used to simulate the progressive post-local buckling of steel tube walls in CFST columns under axial load and fire.

5. Verification of the fiber element model

As discussed in the Introduction, computational and experimental research on the performance of axially-loaded rectangular CFST short columns subjected to fire loading has been very limited. Therefore, experimental data provided by Lu et al [23] and numerical results presented by Yin et al. [34] and Dai and Lam [36] are utilized to verify the fiber element model developed. Lu et al. [23] conducted tests on square CFST short columns at elevated temperatures under constant axial compression. Table 3 provides the details of the specimens. The actual compressive strength of concrete in the tested CFST columns was unknown and usually varies from $0.8f_{cl}^{'}$ to $1.0f_{cl}^{'}$, where $f_{cl}^{'}$ is the compressive strength of concrete cylinder. In the

numerical analyses, $f_c^{'}$ was taken as $0.82 f_{cl}^{'}$. Figure 15 shows the predicted and experimentally measured axial deformation-time relationships. It can be seen that the numerical model generally predicts well the behavior of the tested specimens. However, as shown in Fig. 15a,b and d, experimental fire-resistances are lower than numerical predictions. This is because the actual thermal properties of steel and concrete and moisture content in the columns were not measured in the experiments and the fiber model employed idealized thermal properties of steel and concrete and 3% moisture content in the analyses.

The square CFST short column analyzed by Yin et al. [34] using their analytical model had the width of 443.12 mm and thickness of 17.72 mm. The steel yield strength at ambient temperature was 275 MPa and steel modulus of elasticity was 200000 MPa. The strength of the filled concrete in compression was 25 MPa. The concrete and steel thermal and mechanical properties given in Eurocode 3 [47] were used in the analyses. It was assumed that the contact at the interface of concrete and steel was perfect. The fiber element analysis of the column considered local buckling. The predicted ultimate axial load-exposure time relationship is compared against the solution given by Yin et al. [34] in Fig. 16. It is seen that good agreement between the two numerical solutions is achieved.

Dai and Lam [36] used analysis software ABAQUS to determine the responses of axially loaded short CFST rectangular and square columns under fire. The material and geometric properties of these columns as well as axial loads are provided in Table 4. The steel tube had the Young's modulus of 210000 MPa and yield stress of 350 MPa and filled with 30 MPa concrete. Both the concrete and steel thermal and mechanical properties provided in Eurocode 3 [47] were used. The air gap between the steel tube and concrete was not considered. The predicted fire-resistance of short CFST columns by the fiber model is compared against that obtained by Dai

and Lam in Table 4. It can be observed that there is a good correlation between both numerical predictions. However, the fiber model slightly underestimates the fire-resistance of these CFST short columns. The computed axial displacements as a function of the maximum temperatures on steel tube walls are schematically presented in Figs. 17 and 18 The tube local buckling was not included in the finite element analyses conducted by Dai and Lam [36]. When local buckling was not included in the analyses, the predicted axial displacement-maximum temperature relations by the proposed computational procedure are in good correlation with finite element results. This demonstrates that the influence of local buckling on the fire responses of CFST rectangular short columns is significant.

6. Parametric study

A parametric study was undertaken to explore the behavior of rectangular CFST short columns under combined axial load and fire accounting for the local buckling of steel plates. The parameters examined included the concrete strength, the steel yielding strength, axial load ratio and width-to-thickness ratio. The modulus of elasticity for steel was taken as 210 GPa. The clear width-to-thickness ratios (b / t_s) of the CFST columns used in the following parametric study ranged from 38 to 98 so that the local buckling of these columns was considered in the numerical analyses. In the parametric study, the fiber-based modeling technique was employed to predict either the axial load-strain behavior of CFST short columns subjected to an elevated temperature by increasing the axial strain or the fire-resistance of CFST short columns under constant axial load by increasing the temperature.

6.1. Effects of local buckling

The computer program developed was used to study the influence of local buckling on the performance of short CFST rectangular columns at elevated temperatures. A short rectangular CFST column of 600×500 mm with thickness of 6 mm giving B/t_s and D/t_s ratios of 100 and 83, respectively was employed. The steel yield strength at ambient temperatures was 300 MPa while the concrete had a strength of 40 MPa. The fiber analyses were undertaken on the column exposed to standard fire by including local buckling and excluding its effect, respectively. Figure 19 provides the axial load-strain responses of the CFST column subjected to fire exposure time of 10 minutes, where P_{uo} is the ultimate axial strength of the column at 10 minutes of exposure fire . It is seen that the tube local buckling markedly reduces the column ultimate axial strength by 10.1%. The ultimate axial load-time curves are presented in Fig. 20. At ambient temperature, the reduction in the column ultimate load due to local buckling is 9.2 %. At 20 minutes of fire exposure, the local buckling reduces the column ultimate load by 5.7%. This demonstrates that the effect of local buckling on the ultimate load-carrying capacity of CFST short columns within 20 minutes of fire exposure is significant and its effect diminishes as time increases further.

6.2. Effects of concrete strength

The influences of the concrete strength on the performance of CFST short columns under fire were studied using the fiber model incorporating local buckling. The concrete with compressive strengths of 25, 35, 45 and 55 MPa was used to fill the steel tubes, respectively. The cross-section of the square CFST column was $500\times500\times8.33$ mm with a b/t_s ratio of 58 and f_y = 300 MPa. Figure 21 presents the axial load-strain responses of the short CFST column made of 35 MPa concrete. The column initial stiffness and ultimate strength and decrease significantly with increasing the temperatures. The reductions in the column ultimate strength are 24%,

36%, and 44% when the fire exposure time increases to 20, 40, and 60 minutes, respectively. The influences of the concrete strengths on the ultimate axial load-exposure time curves for CFST columns are shown in Fig. 22. The results show that increasing the strength of concrete significantly increases the column ultimate axial load regardless of the time exposure or temperatures. The column ultimate load could be increased by 24%, 48% and 72% by increasing the concrete strength from 25 MPa to 35MPa, 45MPa and 55 MPa, respectively. At fire exposure time of 10 minutes, the increases in strength of the CFST column are 26%, 53%, and 79% when the compressive strength increases from 25 MPa to 35 MPa, 45 MPa and 55 MPa, respectively. At 20 minutes of fire exposure, the strength increases are 31%, 63, and 94 % by increasing the concrete strength from 25 MPa to 35 MPa, 45 MPa and 55 MPa, respectively. This indicates that the steel tube loses its resistance to fire as time increases and the axial load is transmitted from the steel tube to the filled concrete.

6.3. Effects of steel yield strength

To examine the effects of steel yield strengths at elevated temperatures on the responses of CFST columns under fire, the short rectangular CFST column of 500×400 mm with B/t_s of 50 and D/t_s ratio of 40 was analyzed using the computer program developed. Steel tubes having the yield stresses of 250 MPa, 350 MPa and 450 MPa were considered. Figure 23 shows the axial load–strain responses of the rectangular CFTS short column with yield strength of 450 MPa at different fire exposures times. The column ultimate load-carrying capacity decreases with increasing the fire exposure time. The reductions in the axial stiffness of the short rectangular CFST column are 27%, 48% and 57% when the time exposure increases to 20, 40 and 60 minutes, respectively. The column strength-exposure time curves of CFST columns that had different steel yield stress are provided in Fig. 24. The effect of the yield strength decreases

with increasing the exposure fire time, and its effect vanishes after 40 minutes. At ambient temperature, the column ultimate strength increases by 6%, 12% and 23% respectively when the steel yield stress is increased from 250 MPa to 300 MPa, 350 MPa and 450 MPa. However, at the fire exposure time of 10 minutes, increasing the yield stress of steel from 250 MPa to 300 MPa, MPa, 350 MPa and 450 MPa leads to the column ultimate strength increase by 5%, 10% and 20%, respectively.

6.4. Effects of width-to-thickness ratio

The effects of width-to-thickness ratio on the fire behavior of CFST columns were examined herein. The fiber analyses of a CFST square column of 400×400 mm with B/t_s ratios of 40, 60, 80 and 100 was conducted. The steel tube had a yield stress of 300 MPa and filled with 40 MPa concrete. The axial load-strain-time relationships of the column with B/t_s ratio of 40 are provided in Fig. 25. When the fire exposure time increases to 20, 40 and 60 minutes, the percentage reductions in column ultimate axial strength are 24%, 44%, and 54 %, respectively. Figure 26 demonstrates the effect of B/t_s ratio on the column strength curves at elevated temperatures, where P_{uo} is the ultimate axial strength of the column at ambient temperature for B/t_s 40. It shows that the B/t_s ratio has the most pronounced effect on the column strength at ambient temperature. This effect decreases as the fire exposure time or temperature increases and diminishes after 40 minutes. The column strength at ambient temperature is reduced by 14%, 22% and 26% by increasing the B/t_s ratio from 40 to 60, 80 and 100, respectively. However, at the fire exposure time of 20 minutes, increasing the B/t_s ratio from 40 to 60, 80 and 100 reduces the column strength by 12%, 16%, and 17%, respectively. The smaller the thickness, the faster the heat transfers from the steel to the concrete.

6.5. Effects of axial load ratio

The axial load ratio is computed as the ratio of the applied axial load to the ultimate axial load of a CFST short column at ambient temperature. To study the influences of the loading ratio on fire-resistance of short CFST columns, the fiber model was employed to analyze a square CFST column of 400×400 mm with a B/t_s ratio of 60. The steel tube had a yield stress of 300 MPa was filled with concrete with strength of 40 MPa. The axial load ratio as a function of fire-resistance is given in Fig. 27, where P_{uo} is the ultimate axial strength of the column at ambient temperature. It would appear that the fire-resistance increases significantly with decreasing the axial load ratio. In other words, the axial load has a significant effect on the column fire-resistance. As shown in Fig. 27, when the axial load ratio is 0.92, the fire-resistance obtained is 10 minutes. When the axial load ratio is reduced to 0.64, the fire-resistance increases to 40 minutes. The sharp decline of the column strength is because the steel loses its strength at high temperatures. After 40 minutes, the column strength decreases gradually with increasing the time and the axial load is mainly resisted by the concrete.

6.6. Load distribution

The analysis of a rectangular CFST column of 400×500 mm with thickness of 10 mm was carried out to examine the load distribution in the components of steel and concrete. The concrete with strength of 30 MPa was used to fill the steel tube with yield strength of 300 MPa. The axial loads resisted by the concrete, steel tube and the CFST column as a function of axial strain at the fire exposure time of 10 minutes are illustrated in Fig. 28. The results indicate that at this time of fire exposure, the steel has yielded and its value constant under the applied load. The concrete core shares a significant portion of the ultimate load. The computed contribution

ratios for steel and concrete as a time function are given in Fig. 29. The contribution ratio is defined as $P_{u,s}/P_u$ and $P_{u,c}/P_u$ for steel and concrete, respectively, where $P_{u,s}$, $P_{u,c}$ and P_u are the ultimate axial loads carried by the steel, the concrete and the CFST section, respectively. It can be observed that the steel contribution ratio decreases with an increase in the time exposure or temperature and eventually the steel tube completely loses its strength. In contrast, the concrete contribution ratio increases with increasing the time exposure or temperature and the concrete carries the axial load alone after the steel tube completely loses its capacity.

7. Conclusions

This paper has presented an efficient fiber-based computational model for the fire-resistance simulation of axially-loaded short CFST rectangular columns subjected to fire. The important features including local and post-local buckling, air gap at the interface of concrete and steel tube, concrete moisture content and the emissivity of the exposure surfaces have been considered in the computational modeling technique. The progressive post-local buckling is simulated by the fiber stress redistribution within the buckled steel tube walls using effective width expression derived for steel plates exposed to elevated temperatures. A sequential coupled thermal and nonlinear stress analysis procedure has been developed that calculates the thermal and structural behaviors of CFST columns at elevated temperatures. The computer program implementing the sequential coupled computational procedure has been used to conduct a parametric study on the thermal and structural behavior of rectangular short CFST columns including local buckling effects at elevated temperatures.

The following conclusions are drawn from this research work:

(1) The proposed fiber-based numerical model, which takes into consideration the effects of local buckling, air gap, moisture content and the emissivity of the exposure surfaces, is shown to capture well the fire-resistance of loaded rectangular CFST short columns under standard fire.

(2) Local buckling remarkably reduces the ultimate axial loads of CFST rectangular columns at elevated temperatures and is recommend to be taken into account in numerical modeling techniques.

(3) The ultimate axial load and initial stiffness of CFST short columns decreases significantly as fire exposure time increases.

(4) The higher concrete strength, the higher the ultimate strength of short CFST columns regardless of the fire exposure time.

(5) The steel yield strength has pronounced influences on the axial load-carrying capacities of CFST columns in the first 40 minutes fire exposure.

(6) The B/t_s ratio has a pronounced effect on the column ultimate strengths in fire exposure time of 40 minutes, but its effect diminishes as the time increases.

(7) As the fire exposure time increases, the axial load resisted by the steel tube decreases while the axial load carried by the concrete increases.

References

[1] Furlong RW. Strength of steel-encased concrete beam-columns. J Struct Div ASCE 1967; 93(5):113-124.

[2] Knowles RB, Park R. Strength of concrete-filled steel tubular columns. J Struct Div ASCE 1969;95(12):2565-2587.

[3] Uy B, Bradford MA. Elastic local buckling of thin steel plates in composite steel-concrete members. Eng Struct 1996;18(3):193-200.

[4] Schneider SP. Axially loaded concrete-filled steel tubes. J Struct Eng ASCE 1998; 124(10):1125-1138.

[5] Hajjar JF, Schiller PH, Molodan A. A distributed plasticity model for concrete-filled steel tube beam-columns with interlayer slip. Eng Struct 1998;20(8):663-676.

[6] Uy B. Strength of concrete-filled steel box columns incorporating local buckling. J Struct Eng ASCE 2000;126(3):341-352.

[7] Susantha KAS, Ge HB, Usami T. Uniaxial stress-strain relationship of concrete confined by various shaped steel tubes. Eng Struct 2001;23(10):1331-1347.

[8] Shanmugam NE, Lakshmi B, Uy B. An analytical model for thin-walled steel box columns with concrete in-fill. Eng Struct 2002;24(6):825-838.

[9] Mollazadeh MH, Wang YC. New insights into the mechanism of load introduction into concrete-filled steel tubular column through shear connection. Eng Struct 2014;75:139–151.

[10] AS 3600-2009. Australian Standard for Concrete Structures. Sydney, New South Wales, Australia: Standards Australia, 2009.

[11] Wang, YC. Steel and composite structures: Behaviour and design for fire safety. London and New York: Spon Press, 2002.

[12] Quiel SE, Garlock MEM. Calculating the buckling strength of steel plates exposed to fire. Thin-Wall Struct 2010; 48; 684-695.

[13] Couto C, Real PV, Lopes N, Zhao B. Effective width method to account for the local buckling of steel thin plates at elevated temperatures. Thin-Wall Struct 2014;84:134-149.

[14] Lie TT, Chabot M. Experimental studies on the fire resistance of hollow steel columns filled with plain concrete. Internal report, National Research Council Canada, Institute for Research in Construction, 1992-01.

[15] Sakumoto Y, Okada T, Yoshida M, Tasaka S. Fire resistance of concrete-filled, fire-resiatnt steel-tube columns. J Mat in Civil Eng ASCE 1994;69(2):169-184.

[16] Kodur VKR, Lie TT. Fire performance of concrete-filled hollow steel columns. J Fire Prot Eng 1995;79(3):89-98.

[17] Han LH, Yang YF, Xu L. An experimental study and calculation on the fire resistance of concrete-filled SHS and RHS columns. J Constr Steel Res 2003;59:427-452.

[18] Choi SM, Kim DK, Kim JH, Chung KS, Park SH. Experimental study on fire resistance of concrete-filled steel tube column under constant axial loads. Steel Struct 2005;5(4):305-313.

[19] Han LH, Chen F, Liao FY, Tao Z, Uy B. Fire performance of concrete filled stainless steel tubular columns. Eng Struct 2013;56:165-181.

[20] Espinos A, Romero ML, Serra E, Hospitaler A. Circular and square slender concrete-filled tubular columns under large eccentricities and fire. J Constr Steel Res 2015;110:90-100.

[21] Espinos A, Romero ML, Serra E, Hospitaler A. Experimental investigation on the fire behavior of rectangular and elliptical slender concrete-filled tubular columns. Thin-Wall Struct 2015;93:137-148.

[22] Dundu M. Column buckling tests of hot-rolled concrete filled square hollow sections of mild to high strength steel. Eng Struct 2016; 127:73-85.

[23] Lu H, Zhao XL, Han LH. Fire behaviour of high strength self-consolidating concrete filled steel tubular stub columns. J Constr Steel Res 2009;65:1995-2010.

[24] Lie TT, Chabot M. A method to predict the fire resistance of circular concrete filled hollow steel columns. J Fire Prot Eng 1990;2(4):111-126.

[25] Lie TT, Irwin RJ. Fire resistance of rectangular steel columns filled with bar-reinforced concrete. J Struct Eng ASCE 1995;12(5):797-805.

[26] Kodur VKR, Lie TT. Evaluation of fire resistance of rectangular steel columns filled with fibre-reinforced concrete. Can J Civil Eng 1997;24:339-349.

[27] Han LH. Fire performance of concrete filled steel tubular beam-columns. J Constr Steel Res 2001;57:695-709.

[28] Chung K, Park S, Choi S. Fire resistance of concrete filled square steel tube columns subjected to eccentric axial load. Steel Struct 2009;9:69-76.

[29] Ding J, Wang YC. Realistic modelling of thermal and structural behaviour of unprotected concrete filled tubular columns in fire. J Constr Steel Res 2008;64:1086-1102.

[30] Espinos A, Romero ML, Hospitaler A. Advanced model for predicting the fire response of concrete filled tubular columns. J Constr Steel Res 2010;66:1030-1046.

[31] Hong SD, Varma AH. Analytical modeling of the standard fire behavior of loaded CFT columns. J Constr Steel Res 2009;65:54-69.

[32] Schaumann P, Kodur V, Bahr O. Fire behaviour of hollow structural section steel columns filled high strength concrete. J Constr Steel Res 2009;65:1794-1802.

[33] Wang K, Young B. Fire resistance of concrete-filled high strength steel tubular columns. Thin-Wall Struct 2013;71:46-56.

[34] Yin J, Zha XX, Li LY. Fire resistance of axially loaded concrete filled steel tube columns. J Constr Steel Res 2006;62:723-729.

[35] Song TY, Han LH, Tu HX. Concrete filled steel tube columns under combined temperature and loading. J Constr Steel Res 2010;66:369-382.

[36] Dai XH, Lam D. Shape effect on the behaviour of axially loaded concrete filled steel tubular stub columns at elevated temperature. J Constr Steel Res 2012;73:117-127.

[37] Tao Z, Ghannam M. Heat transfer in concrete-filled carbon and stainless steel tubes exposed to fire. Fire Safety J 2013;61:1-11.

[38] Xion MX, Wang YH, Liew JYR. Evaluation on thermal behaviour of concrete-filled steel tubular columns based on modified finite difference method. Adv in Struct Eng 2016;19(5):746-761.

[39] Ahmed M, Liang QQ, Patel VI, Hadi MNS. Nonlinear analysis of rectangular concrete-filled double steel tubular short columns incorporating local buckling. Eng Struct 2018; 175: 13-26.

[40] Liang QQ. Performance-based analysis of concrete-filled steel tubular beam-columns. Part I: Theory and algorithms. J Constr Steel Res 2009;65(2):363-373.

[41] Liang QQ. Performance-based analysis of concrete-filled steel tubular beam-columns. Part II: Verification and applications. J Constr Steel Res 2009;65(2):351-362.

[42] Liang QQ. Analysis and design of steel and composite structures. Boca Raton and London: CRC Press, Taylor and Francis Group; 2014.

[43] Liang QQ. Nonlinear analysis of circular double-skin concrete-filled steel tubular columns under axial compression. Eng Struct 2017;131:639-650.

[44] Liang QQ. Numerical simulation of high strength circular double-skin concrete-filled steel tubular slender columns. Eng Struct 2018;168:205-217.

[45] Eurocode 1. 1991-1-2, Actions on structures, Part 1.2: General actions- Actions on structures exposed to fire, CEN, Brussels, Belgium, 2002.

[46] Incropera FP, Dewitt DP., Bergman TL, Lavine AS. Fundamental of heat and mass transfer. John Wiley & Sons, 6th Edition, USA 2005.

[47] Eurocode 3. Design of steel structures, Part 1.2: General rules-structural fire design, CEN, Brussels, Belgium, 2005.

[48] Eurocode 2. Design of concrete structures, Part 1.2: General rules-structural fire design, CEN, Brussels, Belgium, 2004.

[49] Liang QQ, Uy B, Liew JYR. Local buckling of steel plates in concrete-filled thin-walled steel tubular beam-columns. J Constr Steel Res 2007;63(3):396-405.

[50] Kamil GM, Liang QQ, Hadi MNS. Local buckling of steel plates in concrete –filled steel tubular columns at elevated temperatures. Eng Struct 2018;168:108-118.

Figures and Tables

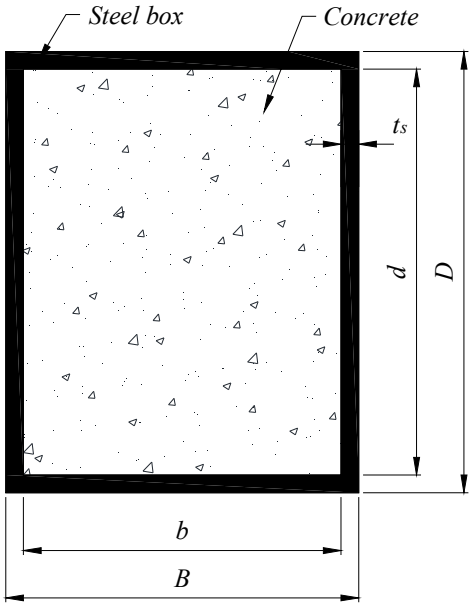

Fig. 1. Cross-section of rectangular CFST column.

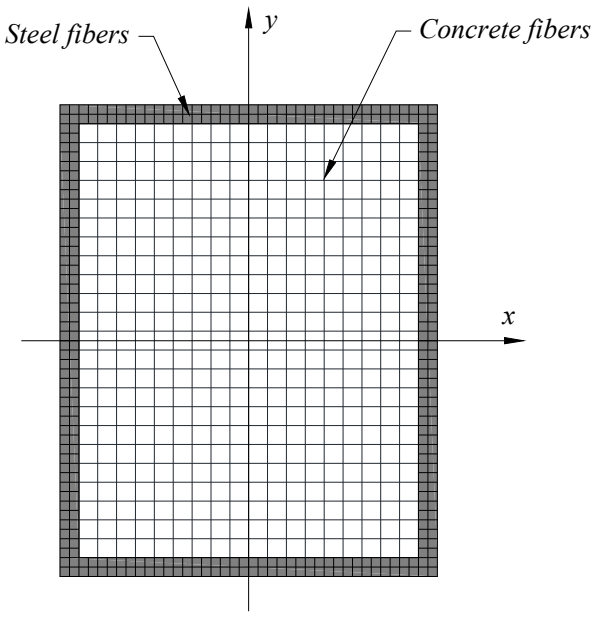

Fig. 2. Typical fibre element discretization.

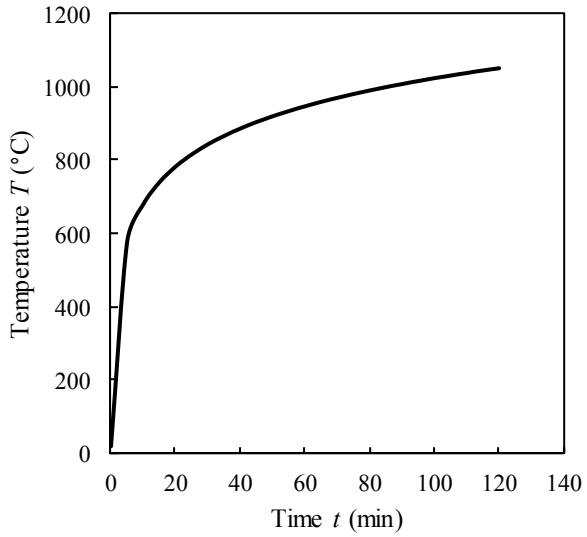

Fig. 3. Standard temperature-Time curve given in Eurocode 1 [43].

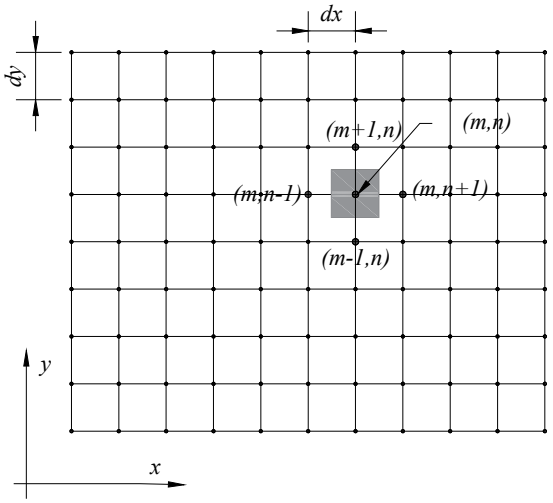

Fig. 4. Nodal grids for the finite difference for temperature analysis

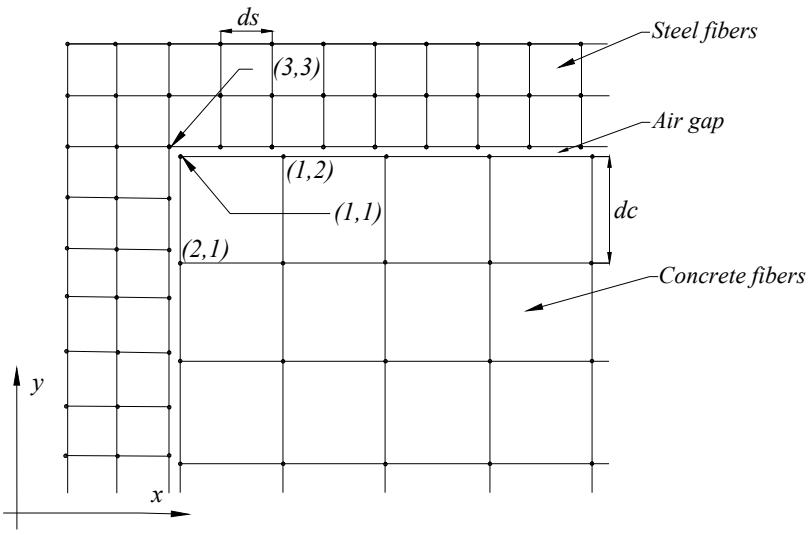

Fig. 5. Typical nodal grids for the interface of steel and concrete for the finite difference temperature analysis

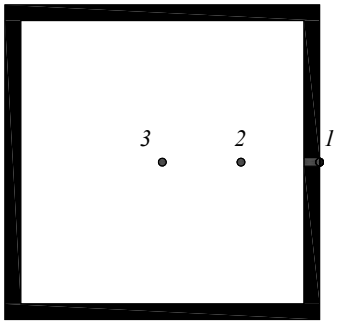

Fig. 6. Point positions in the square CFST column section for comparison purpose.

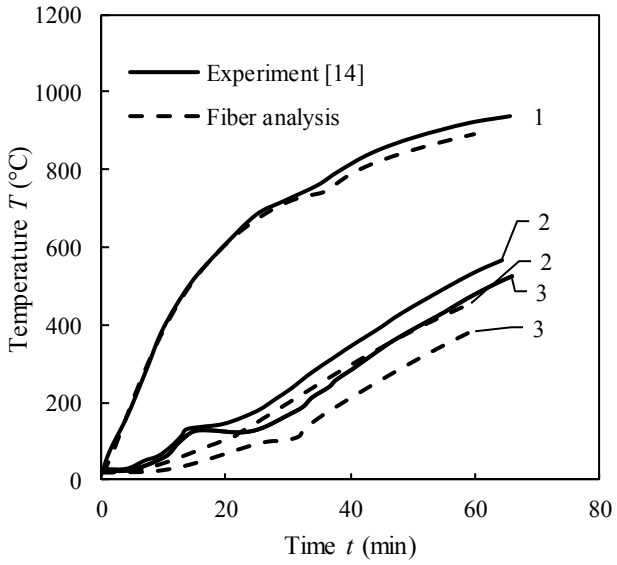

Fig. 7. Comparison of predicted temperatures with experimental results on square CFST column of 152.4×152.4×6.35 mm tested by Lie and Chabot [14].

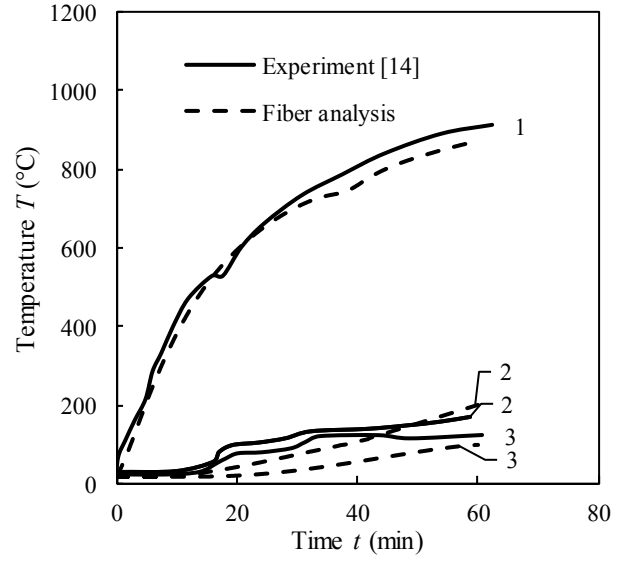

Fig. 8. Comparison of predicted temperatures with experimental results on square CFST column of 254×254×6.35 mm tested by Lie and Chabot [14].

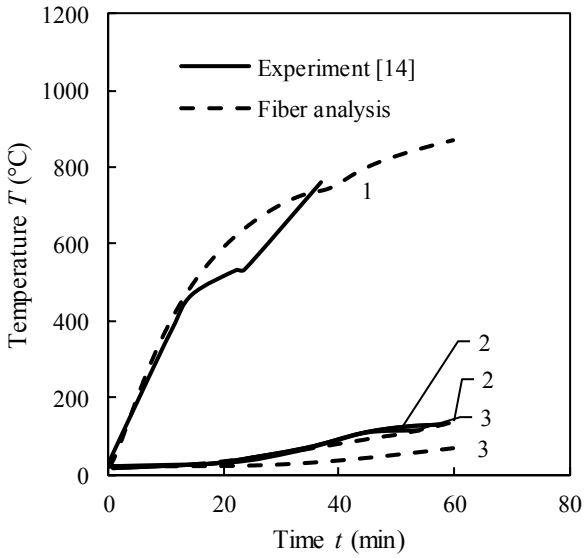

Fig. 9. Comparison of predicted temperatures with experimental results on square CFST column of 304.8×304.8×6.35 mm tested by Lie and Chabot [14].

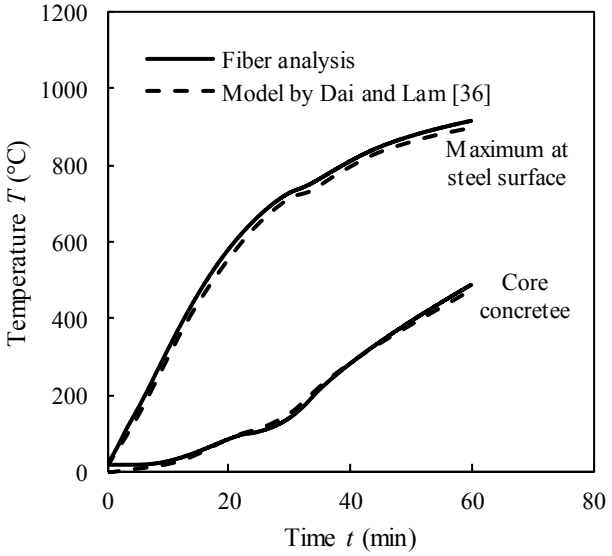

Fig. 10. Comparison of predicted temperatures with finite element results provided by Dai and Lam [36].

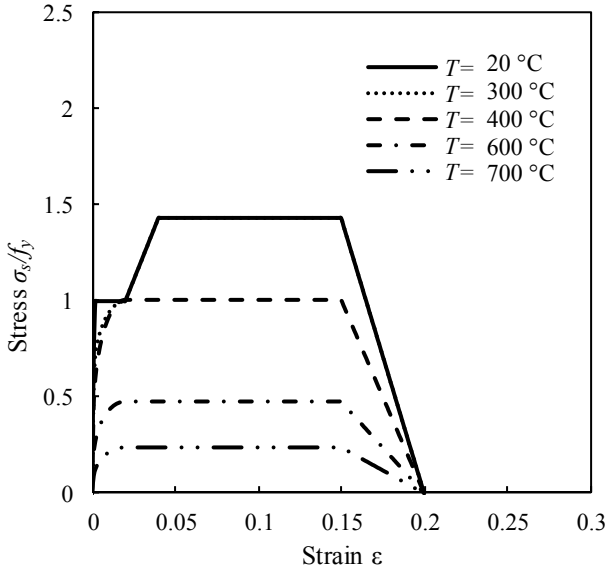

Fig 11. Stress-strain curves for structural steels at elevated temperatures allowing for strain hardening based on Eurocode 3 [47].

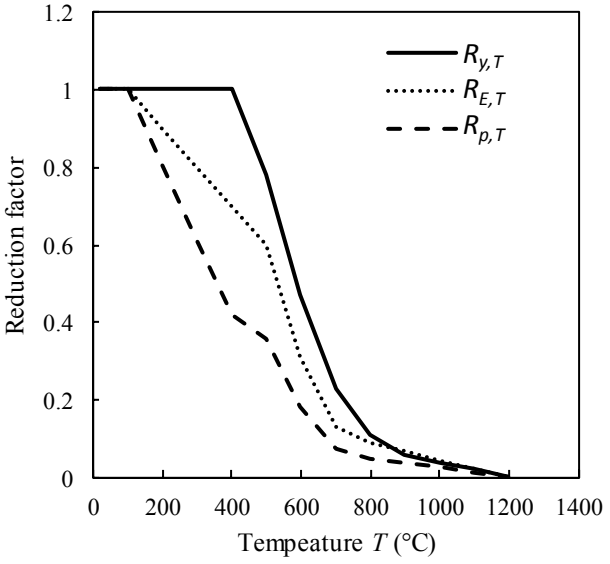

Fig. 12. Reduction factors for the mechanical properties of structural steels at elevated temperatures based on Eurocode 3 [47].

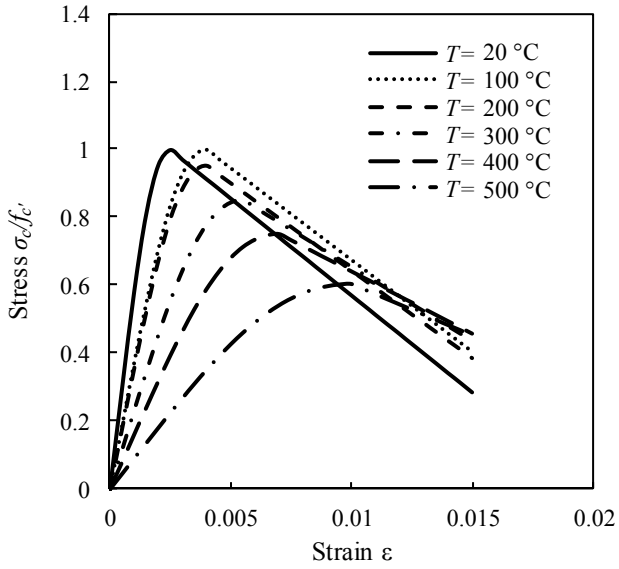

Fig 13. Stress-strain curves for concrete at elevated temperatures based on Eurocode 2 [48].

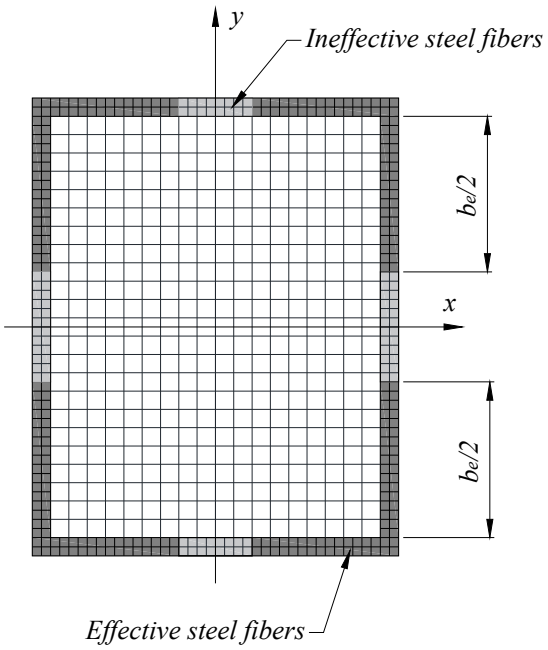

Fig. 14. Effective widths of steel tube walls in rectangular CFST column section.

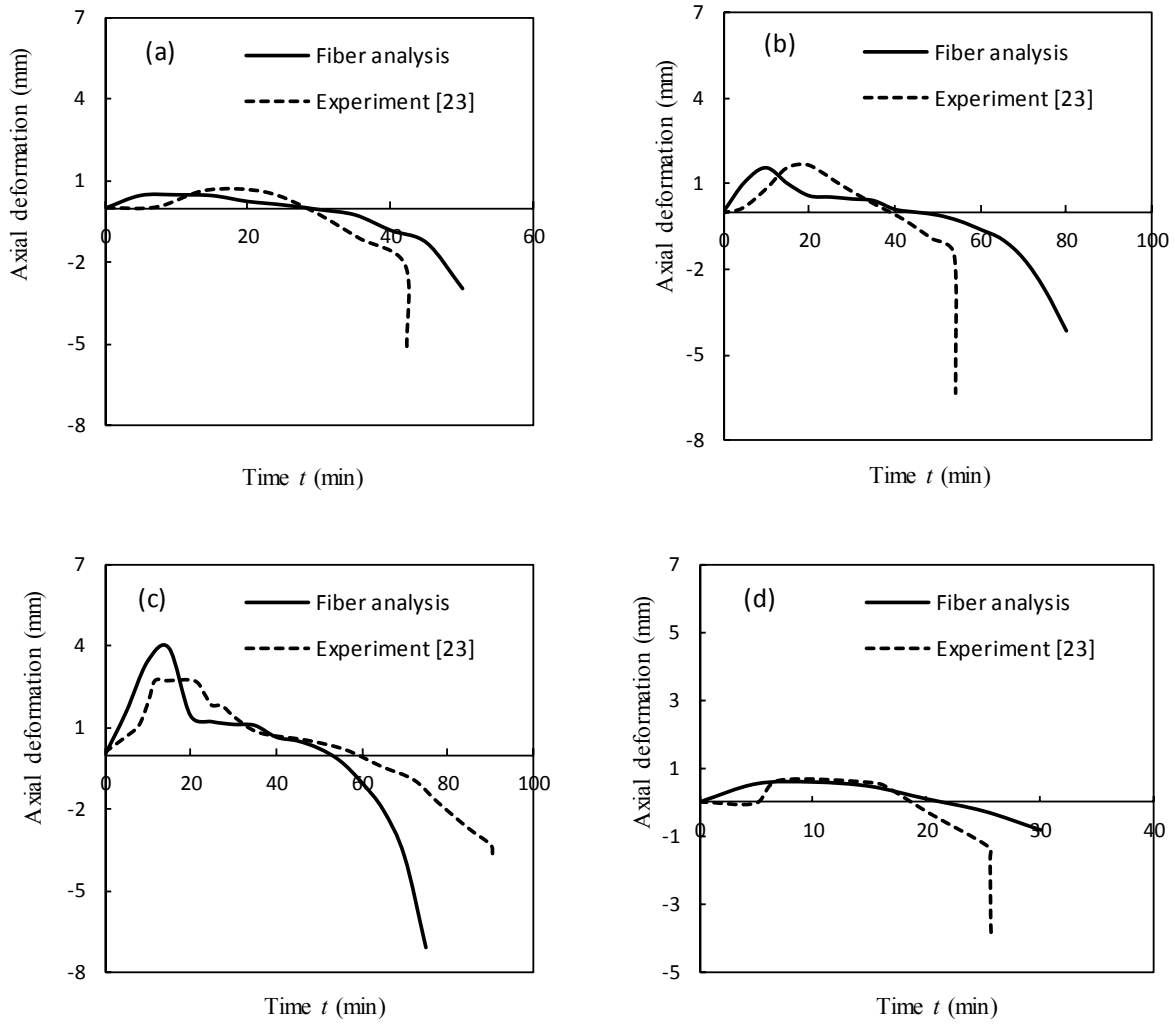

Fig. 15. Comparison of predicted axial displacement-maximum temperature at steel in square CFST short columns tested by Lu et al. [23]: (a) S2R4E0; (b) S2R3E0; (c) S1R2E0; and (d) S1R4E0.

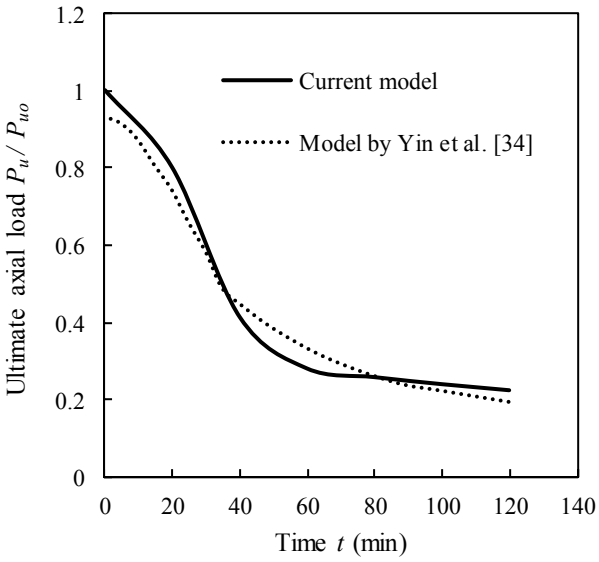

Fig. 16. Comparison of predicted ultimate axial loads with those given by Yin et al. [34].

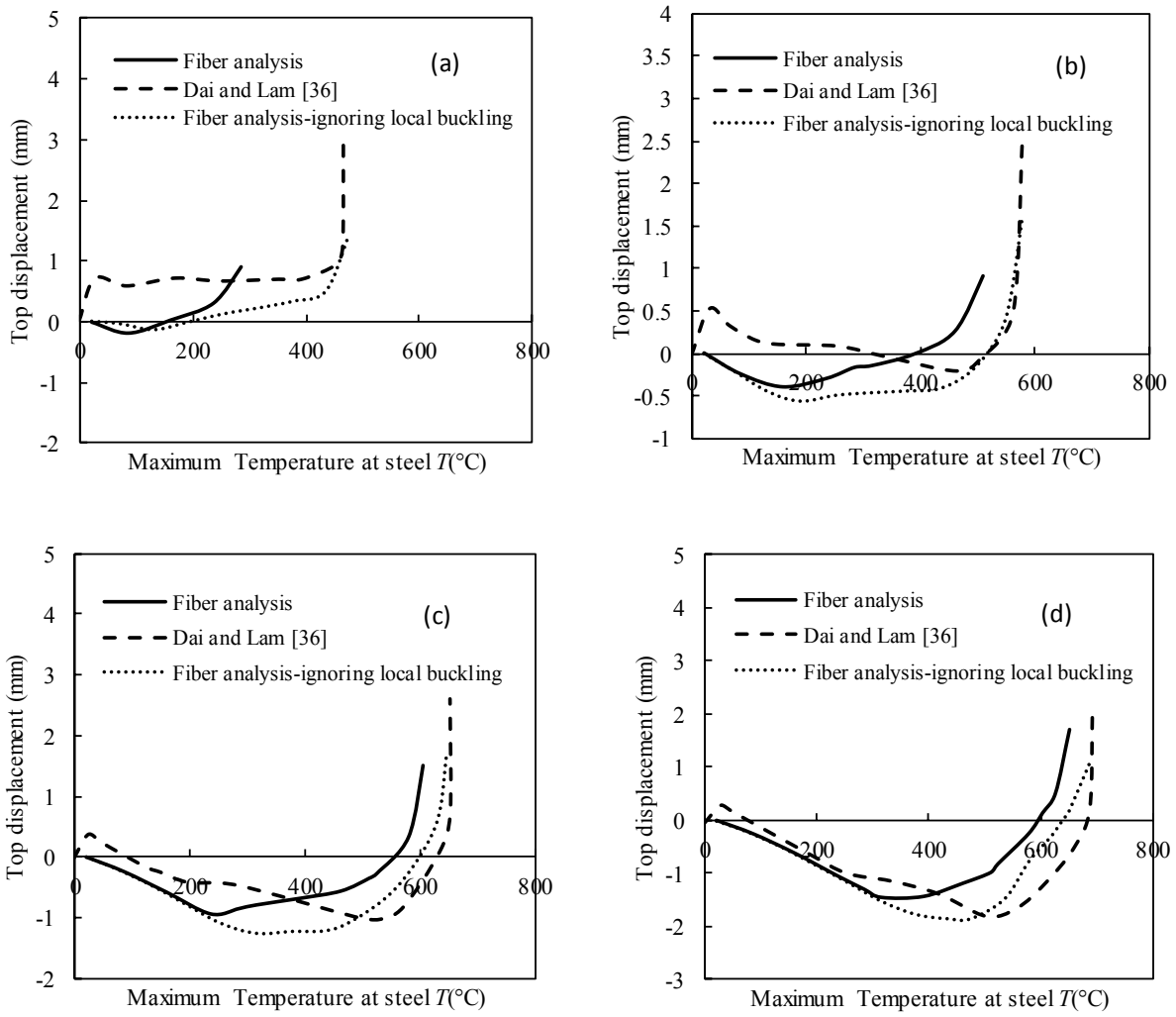

Fig. 17. Comparison of predicted axial displacement-maximum temperature at steel in square CFST short columns those given by Dai and Lam [36]: (a) Axial load=1000 kN ; (b) Axial load=800 kN ; (c) Axial load=600 kN ; and (d) Axial load=500 kN .

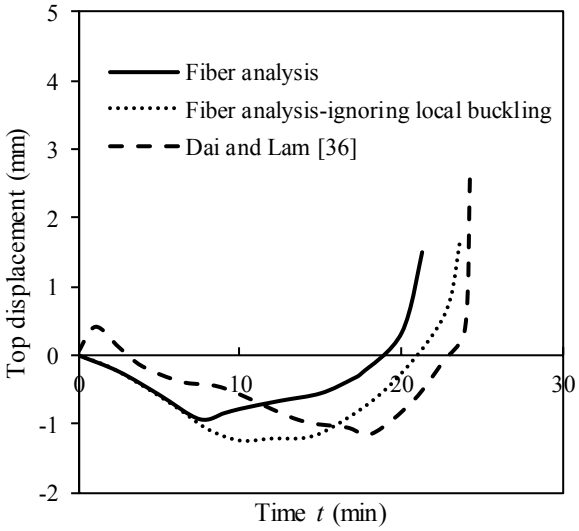

Fig. 18. Comparison of predicted axial displacement-maximum temperature at steel in square CFST short columns with results given by Dai and Lam [36] (axial load= 600 kN).

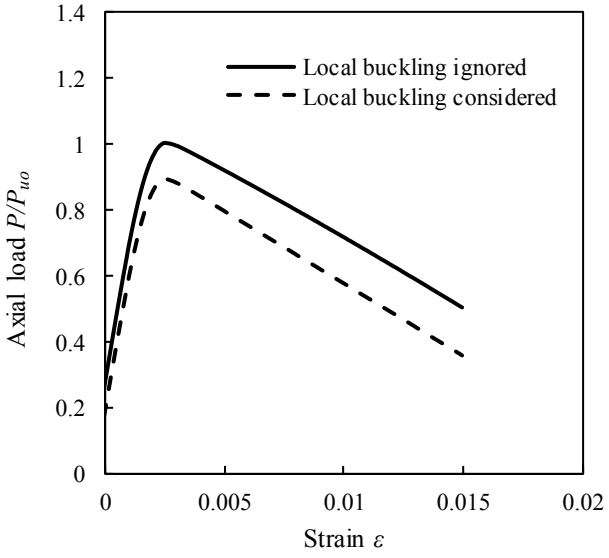

Fig. 19. Influences of local buckling on the axial load-strain behaviour of CFST column subjected to 10 minutes of standard fire.

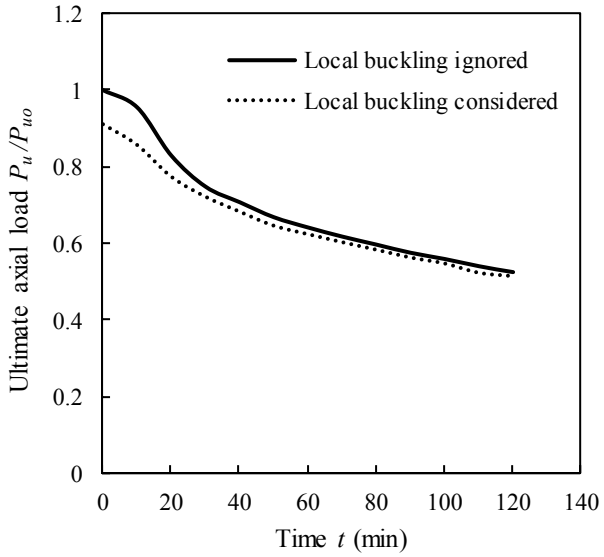

Fig. 20. Influences of local buckling on the ultimate axial strength of CFST column subjected to various time exposure to fire.

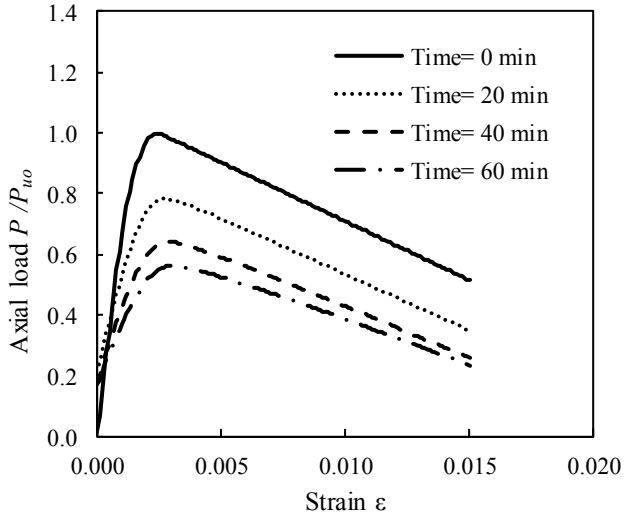

Fig. 21. Axial load-strain curves of square short CFST column with 30 MPa concrete and various fire time exposures.

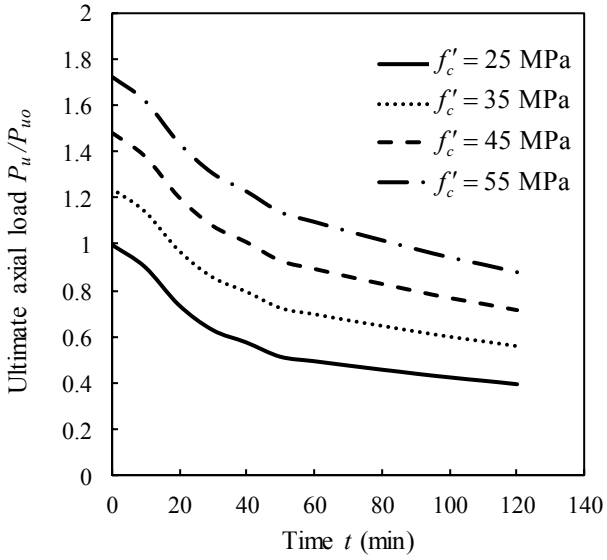

Fig. 22. Effects of concrete strengths on the ultimate strength and fire-resistance of square CFST columns.

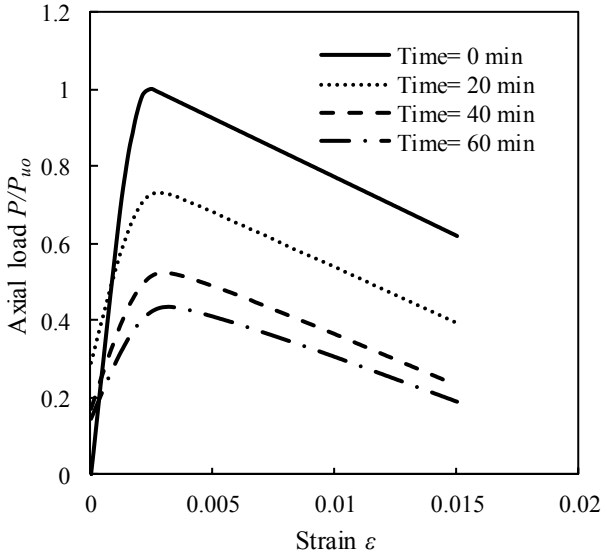

Fig. 23. Axial load-strain curves of rectangular short CFST column with yield strength of 450 MPa exposed to fire.

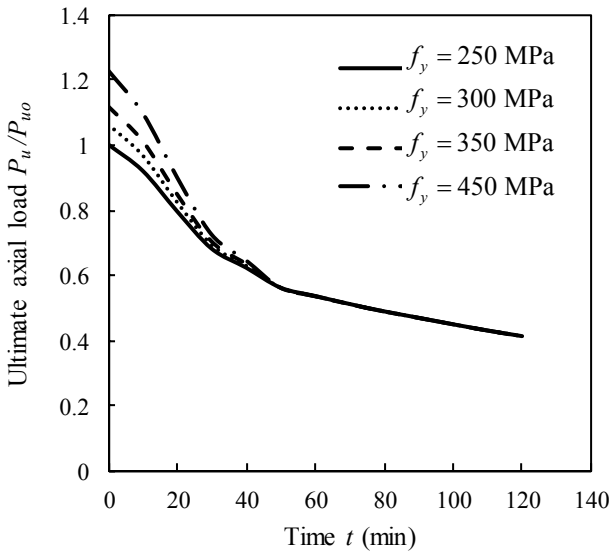

Fig. 24. Effects of the steel yield strength on the ultimate strength of rectangular short CFST columns under fire.

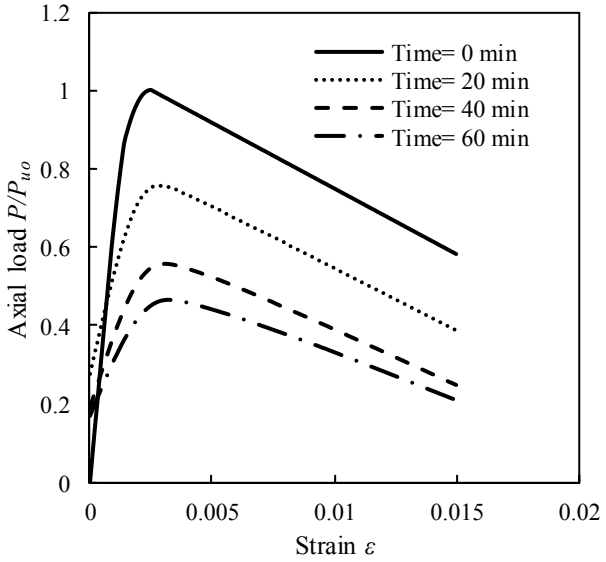

Fig. 25. Axial load-strain relationships of square short CFST column with B/t_s ratio of 60 with various exposure times.

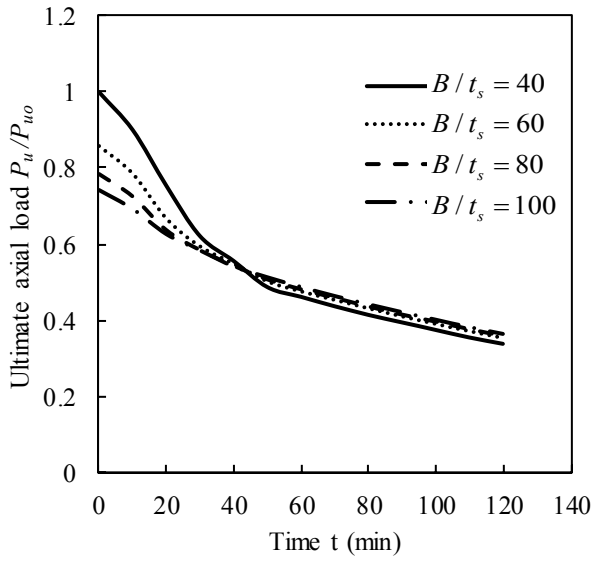

Fig. 26. Ultimate strength of square short CFST column with different B/t_s ratios at different periods of exposure to standard fire.

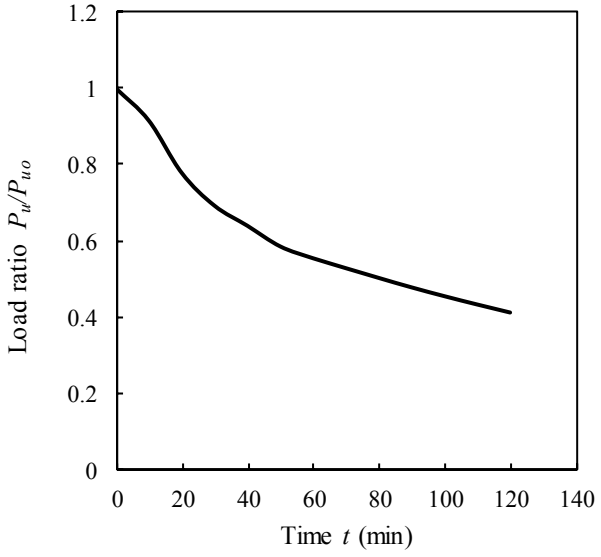

Fig. 27. Load ratio of square short CFST column with B/t_s ratio of 60 at different periods of exposure to standard fire.

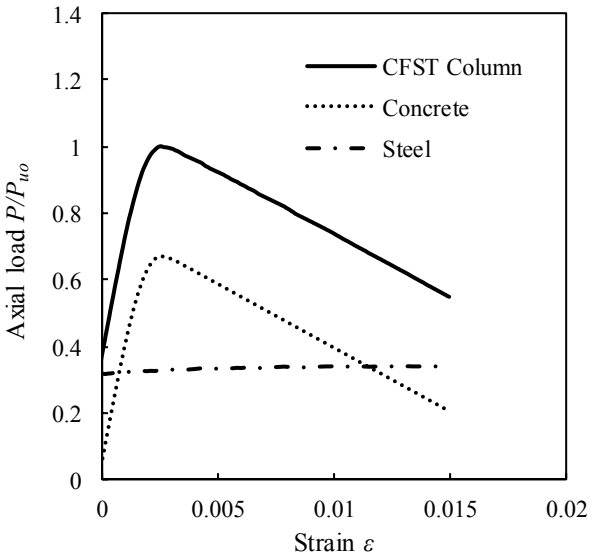

Fig. 28. Load distribution in steel tube and concrete in rectangular short CFST column subjected to 10 minutes fire exposure.

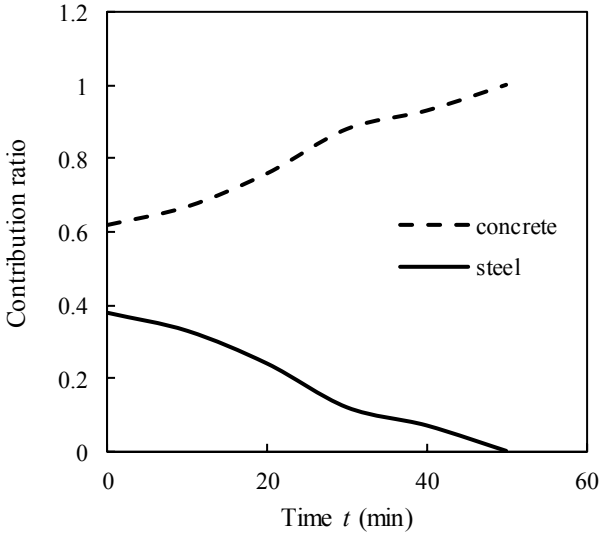

Fig. 29. Steel and concrete contribution ratio as a function of fie exposure time.

Table 1. CFST columns utilized in high-rise buildings

Name of building	City	Column section	Max. size (mm)	*L/r*
LDC Queen's Road Central	Hong Kong	Square	2250×2250	6.5
Di Wang	Shenzhen	Square	1000×1000	14.5
Casselden Place	Melbourne	Circular	950	17.7
The SEG Plazza	Shenzhen	Circular	1600	10.5
The Sail	Singapore	Circular	2000	8.4
The Petronas Tower	Kuala Lumpur	Circular	2400	7.0
Two Union Square	Seattle	Circular	3200	5.3

Table2. Thermal properties of steel and concrete implemented in the numerical model

Materials	Properties	Equations
Steel properties given in Eurocode 3 [48]	Thermal conductivity	$k_{s,T}=\begin{cases}54-3.33\times10^{-2}T & \text{for } 20^{o}C\le T\le 800^{o}C\\ 27.3 & \text{for } 800^{o}C<T\le 1200^{o}C\end{cases}$
	Specific heat	$c_{s,T}=425+7.73\times10^{-1}T-1.69\times10^{-3}T^{2}+2.2\times10^{-6}T^{3}$ for $20°\text{C}\le T\le 600°\text{C}$ $c_{s,T}=666+\frac{13002}{738-T}$ for $600°\text{C}\le T\le 735°\text{C}$ $c_{s,T}=545+\frac{17820}{T-731}$ for $735°\text{C}\le T\le 900°\text{C}$ $c_{s,T}=650$ for $900°\text{C}\le T\le 1200°\text{C}$
	Thermal expansion strain	$\varepsilon_{s,T}=1.2\times10^{-5}T+0.4\times10^{-8}T^{2}-2.416\times10^{-4}$ for $20°C\le T\le 750°C$ $\varepsilon_{s,T}=1.1\times10^{-2}$ for $750°\text{C}\le T\le 860°\text{C}$ $\varepsilon_{s,T}=2\times10^{-5}T-6.2\times10^{-3}$ for $860°\text{C}\le T\le 1200°\text{C}$
Concrete properties given by Lie and Chabot [24]	Thermal conductivity	$k_{c,T}=-0.00085\times T+1.9$ for $0\le T\le 800°\text{C}$ $k_{c,T}=1.22$ for $T>800°\text{C}$
	Thermal capacity	$\rho_c c_{c,T}=(0.005\times T+1.7)\times10^{6}$ for $0\le T\le 200°\text{C}$ $\rho_c c_{c,T}=2.7\times10^{6}$ for $200<T\le 400$ °C $\rho_c c_{c,T}=(0.013\times T-2.5)\times10^{6}$ for $400<T\le 500$ °C $\rho_c c_{c,T}=(-0.013\times T+10.5)\times10^{6}$ for $500<T\le 600$ °C $\rho_c c_{c,T}=2.7\times10^{6}$ for $T>600$ °C
	Thermal expansion strain	$\varepsilon_{c,T}=\left(0.008T+6\right)\times10^{-6}\left(T-20\right)$

Table 3. Dimensions and properties of CFST short columns tested by Lu et al. [23]

Specimen	$B\times D\times t_s$ (mm)	f_y (MPa)	f_u (MPa)	E_s (GPa)	Applied load (kN)
S1R2E0	150×150×5	486	558	197	486
S1R4E0	150×150×5	486	558	197	486
S3R3E0	200×200×6	467	544	199	1226
S2R4E0	200×200×6	467	544	199	1800

Table 4. Comparisons of fire-resistance of CFST short columns

Column	$B\times D\times t_s$ (mm)	Applied load			
		500 kN		600 kN	
		Dai and Lam [35]	Fiber analysis	Dai and Lam [35]	Fiber analysis
		Fire time (min)	Fire time (min)	Fire time (min)	Fire time (min)
SHS	123×123×5	26.955	23.98	25.4	21.26
SHS1	118.9×118.9×5	28.984	22.57	24	20.31
SHS2	125.9×125.9×5	28.069	24.67	26.3	21.8
RHS	169×84.5×5	30.102	23.7	24.91	21.53
RHS1	158.5×79.3×5	26.18	22.43	23.35	20.33
RHS2	179×89.5×5	29.05	25.41	26.88	22.88